Ranking species based on sensitivity to perturbations under non-equilibrium community dynamics

Lucas P Medeiros, Stefano Allesina, Vasilis Dakos, George Sugihara, Serguei Saavedra

Received: 23 February 2022 | Revised: 20 September 2022 | Accepted: 27 September 2022

DOI: 10.1111/ele.14131

ECOLOGY LETTERS cnrs WILEY

METHOD

Ranking species based on sensitivity to perturbations under non-equilibrium community dynamics

Lucas P. Medeiros[1,2] | **Stefano Allesina**[3,4] | **Vasilis Dakos**[5] | **George Sugihara**[6] | **Serguei Saavedra**[1]

[1]Department of Civil and Environmental Engineering, Massachusetts Institute of Technology, Massachusetts, Cambridge, USA

[2]Institute of Marine Sciences, University of California Santa Cruz, California, Santa Cruz, USA

[3]Department of Ecology & Evolution, University of Chicago, Illinois, Chicago, USA

[4]Northwestern Institute on Complex Systems, Northwestern University, Illinois, Evanston, USA

[5]Institut des Sciences de l'Evolution de Montpellier, Université de Montpellier, Montpellier, France

[6]Scripps Institution of Oceanography, University of California San Diego, California, La Jolla, USA

Correspondence
Lucas P. Medeiros, Institute of Marine Sciences, University of California Santa Cruz, Santa Cruz, California, USA.
Email: lumedeir@ucsc.edu

Funding information
DoD-Strategic Environmental Research and Development Program 15, Grant/Award Number: RC-2509; DOI USDI-NPS, Grant/Award Number: P20AC00527; Martin Family Society of Fellows for Sustainability; MIT Sea grant, Massachusetts Institute of Technology; National Science Foundation, Grant/Award Number: ABI-1667584, DEB-1655203 and DEB-2024349

Handling Editor: Frederick Adler

Abstract

Managing ecological communities requires fast detection of species that are sensitive to perturbations. Yet, the focus on recovery to equilibrium has prevented us from assessing species responses to perturbations when abundances fluctuate over time. Here, we introduce two data-driven approaches (expected sensitivity and eigenvector rankings) based on the time-varying Jacobian matrix to rank species over time according to their sensitivity to perturbations on abundances. Using several population dynamics models, we demonstrate that we can infer these rankings from time-series data to predict the order of species sensitivities. We find that the most sensitive species are not always the ones with the most rapidly changing or lowest abundance, which are typical criteria used to monitor populations. Finally, using two empirical time series, we show that sensitive species tend to be harder to forecast. Our results suggest that incorporating information on species interactions can improve how we manage communities out of equilibrium.

KEYWORDS
eigenvector, forecasting, Jacobian matrix, population dynamics, species interactions, time series

INTRODUCTION

Ecological communities are subject to external perturbations such as fires, storms, pollution, and overfishing, which are increasing in magnitude and frequency due to anthropogenic impacts (Barlow et al., 2018; Jackson et al., 2001; Turner et al., 1997). Indeed, strong and frequent perturbations can lead to species extinctions and, as a consequence, to the loss of critical ecosystem services (Cardinale et al., 2012; Levin & Lubchenco, 2008).

In order to avoid the loss of biodiversity and ecosystem services under these circumstances, it is crucial to understand not only the response of the whole community to perturbations but also the response of its constituent species. Individual species may vary in their sensitivity to perturbations—that is, how much their abundance changes after a perturbation—and such sensitivity may be linked to their role in the community (Beauchesne et al., 2021; Dirzo et al., 2014; Estes et al., 2011). For instance, keystone species such as apex predators can be highly sensitive to perturbations and also crucial to maintain community functioning (Estes et al., 2011). Therefore, detecting sensitive species has the potential to greatly improve management and conservation strategies for maintaining community functioning and avoiding biodiversity loss.

Traditional studies in theoretical population ecology have established several important measures of how single species respond to perturbations (Caswell, 2000; Morris & Doak, 2002). Following these developments, indicators such as species abundance or rate of decline are routinely used to characterize the behaviour of populations and determine extinction risks (Mace et al., 2008). More recently, several studies have incorporated information on species interactions to further explore how individual species respond to perturbations (Arnoldi et al., 2018; Beauchesne et al., 2021; Medeiros et al., 2021; Saavedra et al., 2011; Weinans et al., 2019) and, in turn, how individual species can inform us about whole-community changes (i.e. best-indicator or sensor species) (Aparicio et al., 2021; Dakos, 2018; Ghadami et al., 2020; Lever et al., 2020; Patterson et al., 2021). These studies often rely on the assumption of a population dynamics model under a stable equilibrium to which the community returns after a small pulse perturbation on abundances. A pulse perturbation is defined as an instantaneous external shock (e.g. fire, storm) that causes a change in species abundance (Bender et al., 1984; Kéfi et al., 2019). Under this assumption, information on the Jacobian matrix—the matrix containing the local effects of each species on the growth rate of other species and itself (Song & Saavedra, 2021)—can be used to partition the recovery rate of the community into its constituent species (Arnoldi et al., 2018; Ives et al., 1999; Medeiros et al., 2021). A community slightly displaced from equilibrium will asymptotically return along the direction spanned by the leading eigenvector of the Jacobian matrix, that is, the eigenvector associated with the leading (i.e. largest) eigenvalue (Dakos, 2018; Patterson et al., 2021; Strogatz, 2018). Thus, over the short-term, different species may show distinct recovery rates after a perturbation depending on the direction of the leading eigenvector (Arnoldi et al., 2018; Dakos, 2018; Ghadami et al., 2020; Patterson et al., 2021; Weinans et al., 2019). Nevertheless, these ideas cannot be directly applied to communities without a stable equilibrium for which abundances fluctuate over time such as communities with cyclic or chaotic dynamics (Benincà et al., 2009, 2015; Clark & Luis, 2020; Krebs et al., 1995; Sugihara, 1994; Ushio et al., 2018). Moreover, from a practical point of view, it can be unfeasible to monitor how species respond to perturbations using parameterized models given the large amounts of data required to test model assumptions and infer parameters (Bartomeus et al., 2021; Bender et al., 1984).

These limitations raise the question of whether we can measure species responses to perturbations in communities for which dynamics are not at equilibrium. To address this problem, recent methodologies have focused on extracting information directly from abundance time series and measuring how non-equilibrium communities respond to perturbations (Cenci & Saavedra, 2019; Rogers et al., 2022; Ushio et al., 2018). Using a data-driven method known as the S-map to reconstruct the time-varying Jacobian matrix (Deyle et al., 2016; Sugihara, 1994), recent studies have investigated how communities respond to perturbations on abundances (Ushio et al., 2018) and on the governing dynamics (Cenci & Saavedra, 2019). Regarding perturbations on abundances, it has been suggested that the leading eigenvalue of the Jacobian matrix can be used to quantify how communities respond to small perturbations at any given time (Ushio et al., 2018). Differently from a recovery rate in a community with a stable equilibrium, under non-equilibrium dynamics, the leading eigenvalue approximates the local growth rate of small perturbations along a given direction (Eckmann & Ruelle, 1985; Mease et al., 2003; Vallejo et al., 2017). Thus, in contrast to a community at equilibrium with a constant capacity to recover from perturbations, a community under non-equilibrium dynamics has a response to perturbations that depends on how species abundances change over time (i.e. state-dependent) (Cenci & Saavedra, 2019). In particular, the state of a community may determine its response to perturbations not only through the local species' effects on each other (i.e. Jacobian matrix) but also through the local time scale of the dynamics (e.g. perturbation effects may take longer to appear under a long transient) (Hastings et al., 2018; Rinaldi & Scheffer, 2000). Because of such state-dependent behaviour, species abundances have been shown to be harder to forecast, on average, in states where a community is more sensitive to perturbations (Cenci et al., 2020). The question that remains to be answered is whether we can decompose a community's response to monitor the time-varying sensitivity of each of its species and whether this can complement traditional single-species indicators that do not use the information on species interactions. Developing such a species-level measure of response to perturbations could also allow us to test the hypothesis that, as observed for entire communities (Cenci et al., 2020), species that are more sensitive to perturbations at a given state are also harder to forecast.

Here, we develop two complementary approaches based on dynamical systems theory and nonlinear time

series analysis to rank species over time under non-equilibrium dynamics according to their sensitivity to small pulse perturbations on abundances. By doing so, we provide a data-driven framework to detect which species in a community are the most and least sensitive to such perturbations at any given time. Our ranking approaches consist of an analytical measure of the expected sensitivity of each species and an alignment measure of each species with the leading eigenvector of the Jacobian matrix. We test both approaches by performing perturbation analyses using five synthetic time series generated from population dynamics models. We show that we can accurately rank species sensitivities, especially using the expected sensitivity approach. However, the eigenvector approach requires no a priori information about perturbations and performs better when information about perturbations—used to compute expected sensitivities—is biased. Importantly, we show that both approaches remain accurate when inferring the Jacobian matrix directly from the time series with the S-map. Finally, we apply both approaches to two empirical time series and show that species that are more sensitive to perturbations at a given time tend to have larger abundance forecast errors, especially when the local growth rate of perturbations is high.

QUANTIFYING SPECIES SENSITIVITIES TO PERTURBATIONS

To quantify species sensitivities to perturbations, we assume that species abundances in a community with S species change through time according to a generic function: $\frac{d\mathbf{N}}{dt} = \mathbf{f}(\mathbf{N})$, where $\mathbf{f}$ ($\mathbf{f}$: $\mathbb{R}^S \to \mathbb{R}^S$) is an unknown nonlinear model and $\mathbf{N} = \left[N_1, \ldots, N_S\right]^\top$ is the vector of species abundances (Cenci & Saavedra, 2019). At any given time, the community can be affected by a pulse perturbation $\mathbf{p} = \left[p_1, \ldots, p_S\right]^\top$ that changes $\mathbf{N}$ into $\tilde{\mathbf{N}}$ (i.e. $\tilde{\mathbf{N}} = \mathbf{N} + \mathbf{p}$) (Bender et al., 1984). The vector $\tilde{\mathbf{N}}$ would then change in time according to $\mathbf{f}$. Following similar definitions in ecology, we conceptually define sensitivity as the amount of change in species abundances following a perturbation (Dakos, 2018; Domínguez-García et al., 2019). Mathematically, we define the sensitivity of species i to a specific perturbation $\mathbf{p}$ from time t to $t+k$ as the squared difference between its perturbed and unperturbed abundance at the time $t+k$ in relation to the initial squared difference caused by the perturbation at the time t:

$$s_i = \frac{\left[\tilde{N}_i(t+k) - N_i(t+k)\right]^2}{\left[\tilde{N}_i(t) - N_i(t)\right]^2} = \frac{p_i(t+k)^2}{p_i(t)^2}. \quad (1)$$

Therefore, s_i quantifies the distance between perturbed and unperturbed states over time, similarly to measures of sensitivity to initial conditions (Eckmann & Ruelle, 1985; Strogatz, 2018; Vallejo et al., 2017). However, s_i is completely dependent on $\mathbf{p}$. In natural communities, we typically have no prior information about the direction and magnitude of $\mathbf{p}$—that is, there is large uncertainty about how much each species will be affected by a perturbation. To quantify species sensitivity in a way that embraces this uncertainty, we focus on a collection of randomly perturbed abundances (Arnoldi et al., 2018; Bender et al., 1984). Thus, we define the sensitivity of species i from time t to $t+k$ as the average squared difference between a set of n randomly perturbed abundances and its unperturbed abundance at the time $t+k$ in relation to the initial average squared difference at the time t:

$$\langle s_i \rangle = \frac{\frac{1}{n}\sum_{j=1}^{n}\left[\tilde{N}_i^{(j)}(t+k) - N_i(t+k)\right]^2}{\frac{1}{n}\sum_{j=1}^{n}\left[\tilde{N}_i^{(j)}(t) - N_i(t)\right]^2} = \frac{\frac{1}{n}\sum_{j=1}^{n} p_i^{(j)}(t+k)^2}{\frac{1}{n}\sum_{j=1}^{n} p_i^{(j)}(t)^2}, \quad (2)$$

where $\tilde{N}_i^{(j)}(t)$ is the jth perturbed abundance of species i at time t. The denominator in Equation (2) controls for the initial displacement of species abundances but can be ignored if the variance of perturbations is the same for every species (SI Section 4). Note that we use $\langle s_i \rangle$ as a notation for the ratio of the mean squared deviations and that $\langle s_i \rangle$ is greater than zero but not bounded because the numerator may be arbitrarily large.

Under non-equilibrium dynamics, the identity of the most and least sensitive species can change over time. We illustrate this statement using the following 3-species food chain model that exhibits chaotic dynamics (Hastings & Powell, 1991) (parameter values given in SI Section 3):

$$\begin{aligned} \frac{dN_1}{dt} &= rN_1\left(1 - \frac{N_1}{K}\right) - \frac{a_1 N_1 N_2}{1 + b_1 N_1} \\ \frac{dN_2}{dt} &= -sN_2 + hN_1N_2 - \frac{a_2 N_2 N_3}{1 + b_2 N_2} \\ \frac{dN_3}{dt} &= -lN_3 + nN_2N_3, \end{aligned} \quad (3)$$

where N_1, N_2 and N_3 are the abundances of the primary producer, primary consumer, and secondary consumer, respectively. To study species sensitivities under this model, we numerically integrate Equation (3) producing time series (Figure 1a,b) that can be visualized as an attractor in state space (Figure 1c,d). Then, we perform a small arbitrary pulse perturbation $\mathbf{p}$ to species abundances at the time t (orange vertical line in Figure 1a,b) and compute species sensitivities to it $\left(s_i\right)$ after $k = 1$ time step (red vertical line in Figure 1a,b). We use $k = 1$ as an example here, but explore the effects of changing this time step in our analyses. Figure 1a,b shows that even under the same perturbation $\mathbf{p}$, species exhibit drastically different sensitivities depending on when the perturbation occurs. That is, the species that has the largest sensitivity to this

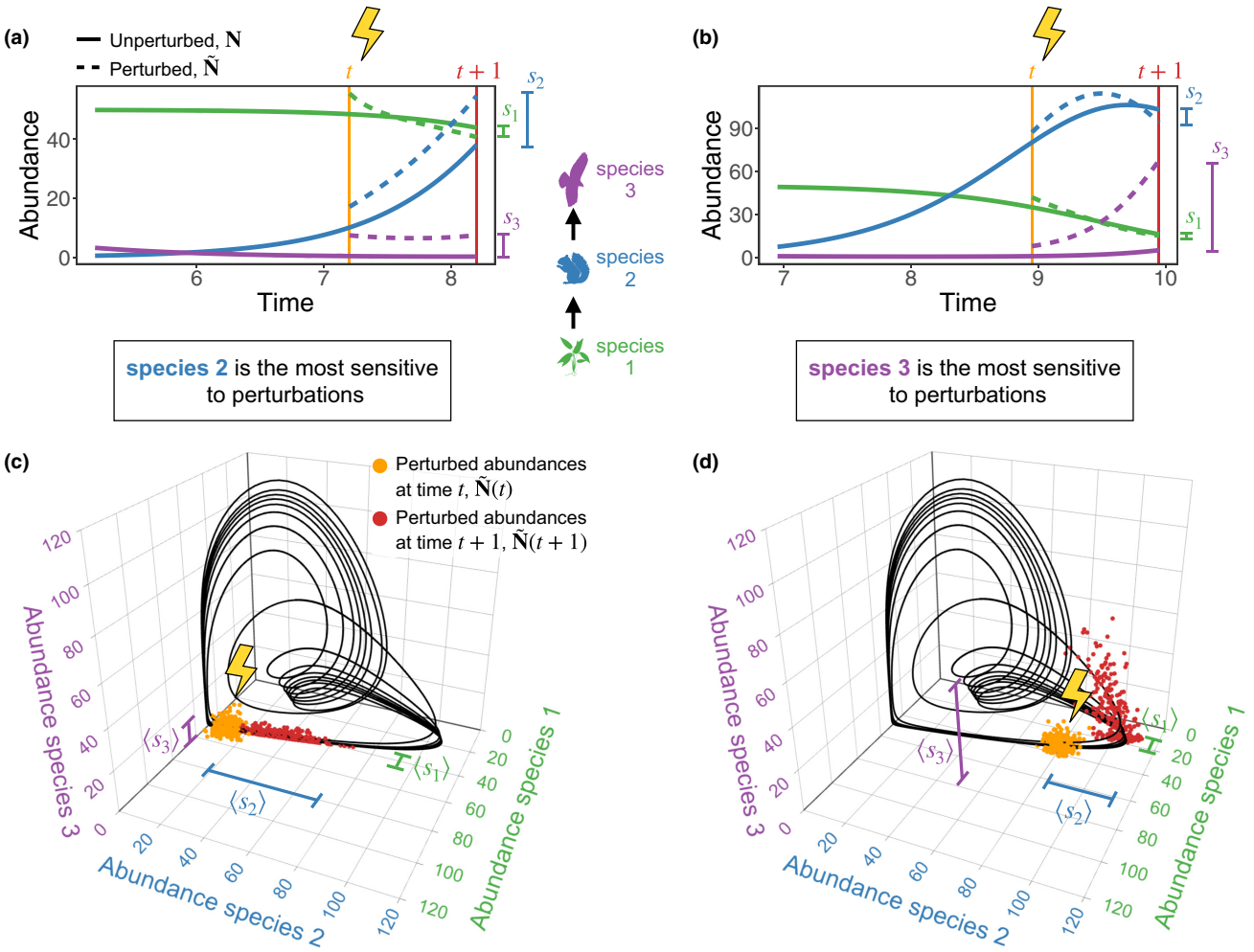

FIGURE 1 Identity of most sensitive species to perturbations changes through time under non-equilibrium dynamics. (a, b) Abundance time series generated from a 3-species chaotic food chain model (Equation 3) showing the effect of a pulse perturbation $\mathbf{p} = [7,7,7]^{\mathsf{T}}$ that increases all abundances at different times t. Whereas species 2 (primary consumer, blue) shows the highest sensitivity s_i to $\mathbf{p}$ (i.e. the largest squared difference between perturbed and unperturbed abundance at $t + 1$) in (a), species 3 (secondary consumer, purple) shows the highest s_i to $\mathbf{p}$ just a few time steps ahead in (b). (c, d) Chaotic attractor of the food chain model (black) with multiple perturbed abundances around $\mathbf{N}(t)$ ($\tilde{\mathbf{N}}(t)$, orange points) at different times t. The red points show these perturbed abundances after one time step ($\tilde{\mathbf{N}}(t + 1)$). We can measure the sensitivity of species i to random perturbations ($\langle s_i \rangle$) by computing the average squared difference between its set of perturbed abundances ($\tilde{N}_i(t + 1)$) and its unperturbed abundance $\left(N_i(t + 1)\right)$ at $t + 1$. Note that this sensitivity measure is normalized by the average squared difference between $\tilde{N}_i(t)$ and $N_i(t)$ at time t (Equation 2). Whereas species 2 shows the highest $\langle s_i \rangle$ in (c), species 3 shows the highest $\langle s_i \rangle$ in (d).

particular perturbation can change from the primary (species 2 in Figure 1a) to the secondary consumer (species 3 in Figure 1b) after a short time. Next, we extend this illustration and consider how multiple randomly perturbed abundances ($\tilde{\mathbf{N}}(t)$, orange points in Figure 1c,d) change after one time step ($\tilde{\mathbf{N}}(t + 1)$, red points in Figure 1c,d) by computing species sensitivities ($\langle s_i \rangle$). Figure 1c,d confirms that the most sensitive species changes from the primary (species 2 in Figure 1c) to the secondary consumer (species 3 in Figure 1d) under random perturbations. Therefore, the problem we aim to solve in this study is how to predict the order of the $\langle s_i \rangle$ values of all species in a community at any given time. Clearly, in natural communities, we cannot produce multiple random perturbations to compare the responses of different species in perturbed and unperturbed communities. Therefore, in what follows, we provide a rationale for using the Jacobian matrix at time t to predict the order of $\langle s_i \rangle$.

RANKING SPECIES SENSITIVITIES TO PERTURBATIONS

Without loss of generality, we can write the linearized dynamics of a small perturbation on abundances as $\frac{d\mathbf{p}}{dt} = \mathbf{J}\mathbf{p}$, where $\mathbf{J}$ is the Jacobian matrix of $\mathbf{f}$ evaluated at $\mathbf{N}$ (SI Section 1) (Boyce et al., 2017; Eckmann & Ruelle, 1985; Mease et al., 2003; Strogatz, 2018). Following results from dynamical systems theory (Arnoldi et al., 2018; Boyce et al., 2017; Strogatz, 2018), we propose two complementary approaches to rank species according to their sensitivity to perturbations (Boxes 1 and 2). These

BOX 1 Expected sensitivity ranking

Rationale

This approach is based on analytically computing an expected value for the sensitivity of species i to perturbations ($\mathbb{E}(s_i)$) using the solution $\mathbf{p}(t+k) = e^{\mathbf{J}k}\mathbf{p}(t)$ of the linearized dynamics (SI Section 2) (Boyce et al., 2017). Note that, for sufficiently small perturbations under equilibrium dynamics, this solution is exact because $\mathbf{J}$ is constant when evaluated at an equilibrium point ($\mathbf{N}^*$ for which $\mathbf{f}(\mathbf{N}^*) = \mathbf{0}$). By assuming that $\mathbf{p}(t)$ follows a distribution with mean zero, we can obtain $\mathbb{E}(s_i)$ at time t from the covariance matrix of $\mathbf{p}(t+k)$: $\mathbf{\Sigma}_{t+k} = e^{\mathbf{J}k}\mathbf{\Sigma}_t\left(e^{\mathbf{J}k}\right)^{\top}$, where $\mathbf{\Sigma}_t$ is the covariance matrix of $\mathbf{p}(t)$. A distribution with a mean zero for $\mathbf{p}(t)$ represents the most uninformative case where all perturbation directions (i.e. which species are most impacted) are equally likely to occur. Thus, the distribution of perturbed abundances ($\tilde{\mathbf{N}}$) described by $\mathbf{\Sigma}_t$ will approximate $\mathbf{\Sigma}_{t+k}$ after k time steps (Figure 2a). Then, we can compute the expected sensitivity of species i as: $\mathbb{E}(s_i) = \sigma^2_{i,t+k}$, where $\sigma^2_{i,t+k}$ is the ith diagonal element of $\mathbf{\Sigma}_{t+k}$ (i.e. the variance of $p_i(t+k)$). We define the order of $\mathbb{E}(s_i)$ values across species as the expected sensitivity ranking and use it to predict the order of species sensitivities to perturbations ($\langle s_i \rangle$; Figure 2a).

Application

Three ingredients are required to apply the expected sensitivity ranking. First, we need the Jacobian matrix of the community ($\mathbf{J}$) evaluated using the abundances ($\mathbf{N}$) at time t. This matrix can be computed directly from a parameterized population dynamics model (SI Section 1) or, as we focus here, inferred from the time series without assuming a specific model (SI Section 5). Second, we need to define an initial covariance matrix of perturbations at time t ($\mathbf{\Sigma}_t$). Without any knowledge of perturbations, we suggest an uninformative approach by setting $\mathbf{\Sigma}_t = \mathbf{I}$, where $\mathbf{I}$ is the identity matrix (i.e. perturbations to each species are independent of each other). Finally, we need to specify the time for which perturbations evolve (k) on the time unit of the time series (e.g. day, month). Because information on the local time scale of the dynamics can be challenging to obtain, we suggest using a small value for k to investigate short-term species sensitivities (e.g. $k = 1$). Alternatively, it is possible to set k to be inversely proportional to the local rate of change calculated from the time series (SI Section 4). In conclusion, although this approach has the advantage of using the information on the entire Jacobian matrix to compute $\mathbb{E}(s_i)$, it has the disadvantage of requiring additional information that may be hard to obtain in natural communities ($\mathbf{\Sigma}_t$ and k).

approaches are based on the assumption that if $\mathbf{J}$ is nearly constant from time t to $t+k$, the solution $\mathbf{p}(t+k)$ of the linearized dynamics provides a good approximation of how perturbed abundances change over this time period. Thus, in addition to the challenge of approximating a nonlinear system (i.e. $\mathbf{f}(\mathbf{N})$) by its linearized dynamics, here we explore the extent to which the linearized dynamics inform us about species sensitivities under non-equilibrium dynamics (i.e. when $\mathbf{J}$ is state-dependent). Importantly, we use information from the Jacobian matrix (i.e. community-level information) to measure how individual species respond to perturbations.

We illustrate how $\mathbb{E}(s_i)$ (Box 1) and $|\,\mathbf{v}_{1i}\,|$ (Box 2) allow us to predict the order of $\langle s_i \rangle$ under three simple scenarios of Lotka-Volterra dynamics at equilibrium (SI Section 13). These examples contain an unstable equilibrium point—that is, $\mathbf{J}$ evaluated at $\mathbf{N}^*$ has at least one $\lambda_i > 0$, as is typically observed for points along a non-equilibrium attractor (e.g. limit cycle, chaotic attractor). We show that the order of $\mathbb{E}(s_i)$ is exactly the same as the order of $\langle s_i \rangle$, whereas the order of $|\,\mathbf{v}_{1i}\,|$ is similar to the order of $\langle s_i \rangle$ for all three scenarios (Figures S1–S3). A potential limitation of these approaches, however, is that they rely on a parameterized model ($\mathbf{f}$) to obtain $\mathbf{J}$, which we rarely have. Therefore, in addition to computing $\mathbb{E}(s_i)$ and $|\,\mathbf{v}_{1i}\,|$ using the analytical $\mathbf{J}$, we show that we can accurately rank $\langle s_i \rangle$ by inferring $\mathbf{J}$ using the S-map. The S-map is a locally weighted state-space regression method that has been shown to provide accurate inferences of the time-varying Jacobian matrix from time series (Cenci et al., 2019; Deyle et al., 2016; Sugihara, 1994) (SI Section 5).

TESTING RANKING APPROACHES WITH SYNTHETIC TIME SERIES

To test whether the order of expected sensitivities ($\mathbb{E}(s_i)$; Box 1) and eigenvector alignments ($|\,\mathbf{v}_{1i}\,|$; Box 2) can predict the order of species sensitivities ($\langle s_i \rangle$), we perform perturbation analyses using synthetic time series. Specifically, we generate multivariate time series with 500 points ($\{\mathbf{N}(t)\}$, $t = 1, \ldots, 500$) using five population dynamics models that produce non-equilibrium dynamics (Figure S5; SI Section 3). Then, for half of each time series ($t = 250, \ldots, 500$), we perform $n = 300$ random perturbations at each time t: $\tilde{\mathbf{N}} = \mathbf{N} + \mathbf{p}$, where $\mathbf{p} \sim \mathcal{N}(\mathbf{0}, \mathbf{\Sigma}_t)$ with $\mathbf{\Sigma}_t$ being a diagonal matrix with diagonal element i

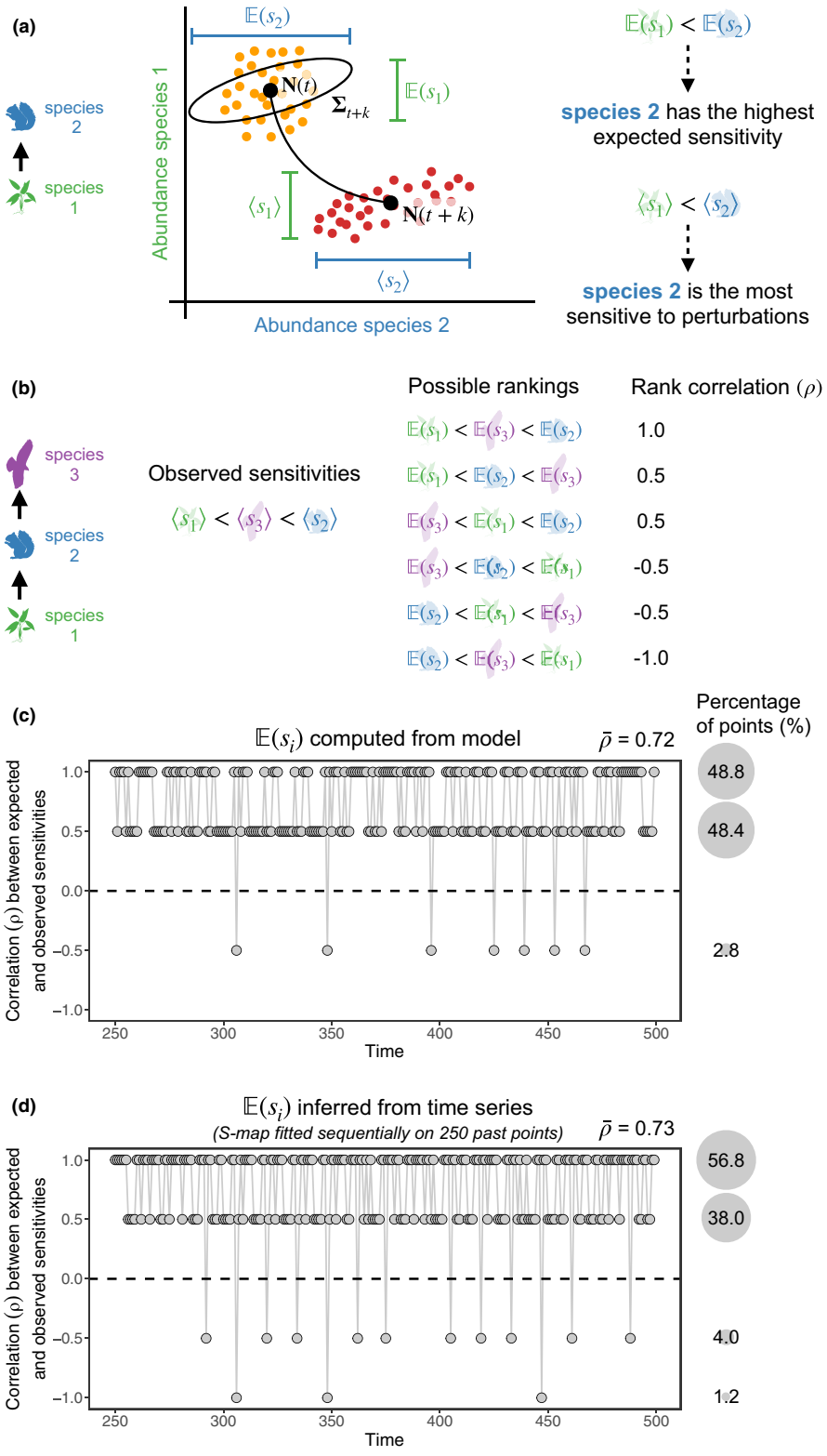

FIGURE 2 Ranking species sensitivities to perturbations. (a) Illustration with two species showing the expansion of perturbed abundances ($\tilde{\mathbf{N}}(t)$, orange points) after k time steps ($\tilde{\mathbf{N}}(t+k)$, red points). The expected sensitivity of species i to perturbations ($\mathbb{E}(s_i)$) can be computed as the corresponding variance of the predicted distribution of perturbations (i.e. ith diagonal element of covariance matrix $\boldsymbol{\Sigma}_{t+k}$ depicted in black). Note that $\boldsymbol{\Sigma}_{t+k}$ is shown at time t as it is computed using only information at that time point. We propose that the order of $\mathbb{E}(s_i)$ values can be used to predict the order of species sensitivities to perturbations ($\langle s_i \rangle$ values). Alternatively, the order of species alignments with the leading eigenvector of the Jacobian matrix ($|\mathbf{v}_{1i}|$ values) can be used to predict the order of $\langle s_i \rangle$ values. (b) for the 3-species food chain model (Equation 3) at a given time, there are six possible ways to rank $\langle s_i \rangle$ values, each one giving a Spearman's rank correlation value (ρ). (c) Rank correlation (ρ) between $\mathbb{E}(s_i)$ (computed analytically from the model) and $\langle s_i \rangle$ over time quantified for a synthetic time series generated from the 3-species food chain model. The vast majority of points (97.2%) show a positive ρ. (d) Same as (c) but with the Jacobian matrix used to compute $\mathbb{E}(s_i)$ inferred with the S-map using only past time-series data. Again, the great majority of points (94.8%) show a positive ρ.

BOX 2 Eigenvector ranking

Rationale

This approach is based on the alignment of species i with the leading eigenvector ($\mathbf{v}_1$) of $\mathbf{J}$ | $\mathbf{v}_{1i}$ |. The solution of the linearized dynamics can also be written as $\mathbf{p}(t+k) = \sum_{i=1}^{S} c_i e^{\lambda_i k}\mathbf{v}_i$, where $\mathbf{v}_i$ is the real part of the ith eigenvector of $\mathbf{J}$, λ_i is the real part of the ith eigenvalue $\left(\lambda_S \leq \cdots \leq \lambda_1\right)$, and each c_i is a constant determined by the initial condition $\mathbf{p}(t)$ (SI Section 9) (Boyce et al., 2017, Strogatz, 2018). As long as the imaginary parts are small compared to real parts, | $\mathbf{v}_{1i}$ | can still be used to estimate species sensitivities even under small local oscillations caused by complex eigenvalues (SI Section 9). After a sufficient amount of time k, λ_1 will dominate over other eigenvalues and the solution can be approximated by $\mathbf{p}(t+k) \approx c_1 e^{\lambda_1 k}\mathbf{v}_1$. Thus, $\mathbf{v}_1$ dictates the local direction of the greatest expansion (or smallest contraction) of perturbations. That is, the distribution of perturbed abundances ($\tilde{\mathbf{N}}$) will expand over time approximately along the direction of $\mathbf{v}_1$ and at a rate given by λ_1 (positive values lead to expansion, whereas negative values lead to contraction). We also show that $\mathbf{v}_1$ serves as a proxy for the local leading Lyapunov vector, which provides the exact direction of perturbation growth under non-equilibrium dynamics (Kuptsov & Parlitz, 2012; Mease et al., 2003; Vallejo etal., 2017) (Figure S4; SI Section 10). Specifically, we compute the alignment of species i with $\mathbf{v}_1$ as the absolute value of its ith element (| $\mathbf{v}_{1i}$ |), where $\|\mathbf{v}_1\| = 1$. We define the order of | $\mathbf{v}_{1i}$ | values across species as the eigenvector ranking and use it to predict the order of $\langle s_i \rangle$ (SI Section 11). Note that we use the absolute value because only the line spanned by $\mathbf{v}_1$ and not its direction determines how perturbed abundances change over time.

Application

Similarly to the expected sensitivity ranking, the Jacobian matrix of the community ($\mathbf{J}$) evaluated using the abundances ($\mathbf{N}$) at time t is also required to apply the eigenvector ranking. The main advantage of the eigenvector ranking is that $\mathbf{J}$ is the only ingredient required to compute | $\mathbf{v}_{1i}$ | and we do not need to specify the initial covariance matrix of perturbations ($\mathbf{\Sigma}_t$) nor the time for which perturbations evolve (k). Nevertheless, using a single eigenvector instead of the entire Jacobian matrix, the eigenvector ranking uses less information than the expected sensitivity ranking. Importantly, we show that $\mathbb{E}\left(s_i\right)$ and | $\mathbf{v}_{1i}$ | are related in the special case of a symmetric $\mathbf{J}$ (SI Section 12), which is also when all eigenvalues of $\mathbf{J}$ are real.

given by $\sigma^2_{i,t} = r^2$ (i.e. independent normally distributed perturbations for each species with the same variance r^2). We set r to be 15% of the mean standard deviation of species abundances, but relax this assumption in additional analyses (SI Section 4). Next, we numerically integrate the model $\mathbf{f}$ for a time k using each $\tilde{\mathbf{N}}$ as an initial condition. Because the response of communities to perturbations can depend on the time scale of the dynamics (Hastings et al., 2018; Rinaldi & Scheffer, 2000), we set k to be inversely proportional to the mean rate of change of the dynamics (SI Section 4). Then, we compute $\langle s_i \rangle$ from time t to $t+k$ as well as $\mathbb{E}\left(s_i\right)$ and | $\mathbf{v}_{1i}$ | using $\mathbf{J}$ at time t as described in Boxes 1 and 2. We compute $\mathbb{E}\left(s_i\right)$ and | $\mathbf{v}_{1i}$ | both analytically from the true $\mathbf{J}$ evaluated at $\mathbf{N}$ and by sequentially inferring $\mathbf{J}$ with the S-map on 250 past points.

To assess how well the order of $\mathbb{E}\left(s_i\right)$ and | $\mathbf{v}_{1i}$ | predicts the order of $\langle s_i \rangle$, we compute the Spearman's rank correlation (ρ) between each ranking and $\langle s_i \rangle$ at each time t. We focus on predicting the order instead of the exact values of $\langle s_i \rangle$ for two reasons. First, the exact values of $\langle s_i \rangle$ depend on the initial covariance matrix $\mathbf{\Sigma}_t$ and on the time step k, which we rarely know for natural communities. Second, we can only infer an approximation of $\mathbf{J}$ with the S-map even from ideal time-series data (SI Section 5; Cenci & Saavedra, 2019). We can illustrate our ranking procedure for $\mathbb{E}\left(s_i\right)$ by considering the 3-species food chain model (Figure 1; Equation 3). With 3 species, there are 6 possible ways to rank a given set of $\langle s_i \rangle$ at any given time, resulting in 4 different ρ values (Figure 2b). If the order of $\mathbb{E}\left(s_i\right)$ matches the order of $\langle s_i \rangle$ exactly, we obtain $\rho = 1$ (Figure 2b). Otherwise, ρ decreases depending on the mismatch between the order of $\mathbb{E}\left(s_i\right)$ and the order of $\langle s_i \rangle$. An advantage of using ρ is that it allows us to penalize prediction mistakes consistently, irrespective of whether the mistaken species are amongst the most or least sensitive ones. For example, in Figure 2b, the second and third rankings have because both contain one correct prediction, which is the least sensitive species and the most sensitive species, respectively. Under the 3-species food chain model, we find that the order of matches the order of $\langle s_i \rangle$ exactly (i.e. $\rho = 1$; Figure 2c) for 48.8% of points in the time series. For another 48.4% of points, the order of $\mathbb{E}\left(s_i\right)$ allows us to correctly detect the position of either the least or most sensitive species (i.e. $\rho = 0.5$). Finally, for 2.8% of points, the order of $\mathbb{E}\left(s_i\right)$ is not a good predictor of the order of $\langle s_i \rangle$ (i.e. $\rho < 0$). But most strikingly, we obtain very similar results when inferring $\mathbb{E}\left(s_i\right)$ directly from the synthetic time series using the S-map, without any knowledge of the underlying model (Figure 2d). Hence, this illustration suggests that we can accurately predict the relative

sensitivity position of most species (i.e. $\rho \geq 0.5$) for the vast majority of points in a time series.

To benchmark our approaches, we use two simple single-species indicators to predict the order of $\langle s_i \rangle$ values. First, we use abundances absolute percent change between $t-1$ and t: $\Delta N_i(t) = \left| \frac{N_i(t) - N_i(t-1)}{N_i(t-1)} \right|$. The rationale for this indicator is that a species will be more sensitive when its abundance is changing more rapidly. Second, we use abundances at time t after a sign reversal: $-N_i(t)$. This indicator is based on the notion that a species will be more sensitive when it has a low abundance, for example, due to density dependence effects. For both indicators, we compute the rank correlation ρ between $\langle s_i \rangle$ and the indicator at each time t. Note that computing $\Delta N_i(t)$ or $-N_i(t)$ for a given species i only requires species-level information (i.e. time series of species i) and not community-level information (i.e. Jacobian matrix) as $\mathbb{E}(s_i)$ and $|\mathbf{v}_{1i}|$ require.

We demonstrate the generality of our ranking approaches using the set of five synthetic time series (SI Section 3). Although we find a high variation in ρ over time (grey points in Figure 3a), the mean correlation $\overline{\rho}$ between $\langle s_i \rangle$ and $\mathbb{E}(s_i)$ as well as between $\langle s_i \rangle$ and $|\mathbf{v}_{1i}|$ is positive and high for all five models when we compute these rankings from the model (horizontal lines in Figure 3a). In particular, we find that $\mathbb{E}(s_i)$ shows the higher accuracy in ranking $\langle s_i \rangle$, followed by $|\mathbf{v}_{1i}|$, $\Delta N_i(t)$, and $-N_i(t)$. Note that we focus on $\overline{\rho}$ given that ρ is expected to vary over time due to changes in nonlinearity and rate of change of $\mathbf{J}$. Importantly, we obtain very similar results for all models when inferring $\mathbb{E}(s_i)$ and $|\mathbf{v}_{1i}|$ using the S-map (horizontal lines in Figure 3b). In addition to quantifying prediction accuracy, we can visualize how the value of $\langle s_i \rangle$, $\mathbb{E}(s_i)$, and $|\mathbf{v}_{1i}|$ of each species changes over time (Figure S6). We find that, even when inferring $\mathbb{E}(s_i)$ and $|\mathbf{v}_{1i}|$ with the S-map, we are able to detect shifts in $\langle s_i \rangle$ across species (Figure S6).

Although $\mathbb{E}(s_i)$ is in general more accurate than $|\mathbf{v}_{1i}|$, we can use information on the leading eigenvalue (λ_1) to increase the accuracy of the latter approach. We expect that the higher λ_1, the greater the local growth rate of perturbations in the direction of $\mathbf{v}_1$, which should improve our ability to rank $\langle s_i \rangle$ using $|\mathbf{v}_{1i}|$. For the non-equilibrium attractors used here, λ_1 is generally positive, whereas subsequent eigenvalues are negative or close to zero, implying that λ_1 alone carries enough information to improve the eigenvector approach. Indeed, we find that $\overline{\rho}$ generally increases for the eigenvector approach when using only a subset of points with a high value of λ_1 (Figure S7). We also find a positive correlation between the analytical and inferred λ_1 (2-species predator–prey: 0.52; 3-species food chain: 0.70; 3-species food web: 0.57; 4-species competitors: 0.23; and 5-species food web: 0.70) and a high alignment between the analytical and inferred $\mathbf{v}_1$ for all models (Figure S8).

For most models, the expected sensitivity ($\mathbb{E}(s_i)$) and eigenvector ($|\mathbf{v}_{1i}|$) approaches computed from the analytical $\mathbf{J}$ show a high accuracy in ranking species sensitivities ($\langle s_i \rangle$) when using different perturbation distributions (Figures S9 and S10) or time steps (k) to evolve perturbations (Figures S11 and S12; SI Section 4). In particular, $\mathbb{E}(s_i)$ shows an extremely high accuracy when k is small and fixed over time (e.g. $k = 1$; Figure S11), given that the solution for the linearized dynamics ($\mathbf{p}(t+k)$) is more precise for smaller k. In contrast, we find that $|\mathbf{v}_{1i}|$ performs best when k depends on the time scale of the dynamics (Figure 3), given that the eigenvector approach depends on the convergence of $\mathbf{p}(t+k)$ to the line spanned by $\mathbf{v}_1$, which requires a larger k when dynamics are slower. We also find that the accuracy of $\mathbb{E}(s_i)$ computed using wrong values of k and $\mathbf{\Sigma}_t$ remains high (Figures S10 and S13), except when these values are greatly misspecified (Figure S14). Finally, although the accuracy decreases in some cases, we find that $\mathbb{E}(s_i)$ and $|\mathbf{v}_{1i}|$ inferred with the S-map remain accurate when normalizing species abundances (Figure S15), using shorter time series (Figure S16), adding observational noise to the time series (Figure S17) or adding process noise to the model (Figure S18; SI Section 6).

DETECTING SENSITIVE SPECIES IN EMPIRICAL TIME SERIES

To illustrate the implementation of our data-driven approaches, we apply them to rank species sensitivities (Boxes 1 and 2) using two empirical time series. Each time series depicts a different marine community with four interacting variables that have been shown to exhibit non-equilibrium dynamics (SI Section 7; Benincà et al., 2009, 2015). Note that some variables represent physical attributes (e.g. bare rock) and others consist of species aggregations (e.g. barnacles) but we use the term species to refer to all variables. We first fit the S-map sequentially to both time series to infer $\mathbb{E}(s_i)$ and $|\mathbf{v}_{1i}|$ (SI Section 7). Because we do not know the governing population dynamics in these communities (i.e. $\mathbf{f}(\mathbf{N})$), we cannot compute $\langle s_i \rangle$. Instead, we perform abundance forecasts using a Long Short-Term Memory (LSTM) neural network (James et al., 2021) and test the hypothesis that species that are more sensitive to perturbations (i.e. have a higher value of $\mathbb{E}(s_i)$ or $|\mathbf{v}_{1i}|$) at a given time will be harder to forecast. That is, for a community under perturbations, the LSTM neural network will not be able to accurately forecast the abundance of a given species at a point in time when that species is highly sensitive to perturbations (Cenci et al., 2020). Both empirical communities described above are thought to be under perturbations triggered by changes in environmental conditions (Benincà et al., 2009, 2015).

For both the Jacobian matrix inference (i.e. S-map) and the forecasts (i.e. LSTM neural network), we assign 70% of the data as a training set and use the remaining 30% as a test set. For each time t in the test set, we

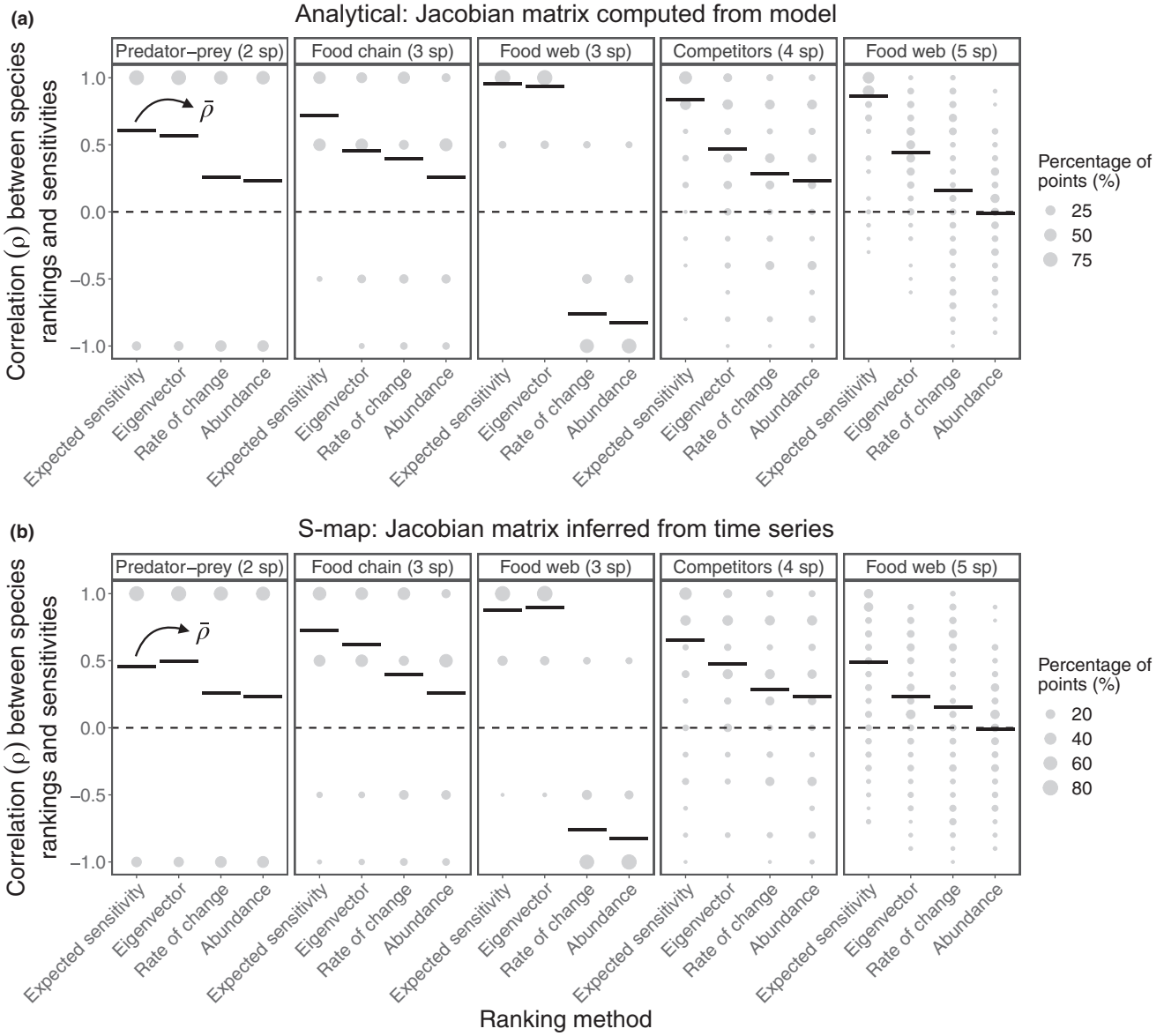

FIGURE 3 Expected sensitivity and eigenvector approaches allow us to accurately rank species sensitivities to perturbations under several population dynamics models. (a) Rank correlation (ρ) between species sensitivities to perturbations ($\langle s_i \rangle$) and four different approaches (expected sensitivity, $\mathbb{E}(s_i)$; eigenvector, $|\mathbf{v}_{1i}|$; rate of change, $\Delta N_i(t)$; and abundance, $-N_i(t)$). Note that the Jacobian matrix and, therefore, $\mathbb{E}(s_i)$ and $|\mathbf{v}_{1i}|$ are computed analytically from the model. Each panel shows the percentage of points with a given ρ value (size of grey points) and the average of these values across time ($\bar{\rho}$, black horizontal lines) for a synthetic time series generated from the corresponding population dynamics model. (b) Same as (a) but with the Jacobian matrix and, therefore, $\mathbb{E}(s_i)$ and $|\mathbf{v}_{1i}|$ inferred with the S-map using only past time-series data. In (a), the expected sensitivity approach shows a higher $\bar{\rho}$ than the other three ranking approaches under all models. In (b), the expected sensitivity approach outperforms the eigenvector approach for three out of five models.

compute a standardized forecast root-mean-square error (RMSE) for each species i as (Perretti et al., 2013):

$$\varepsilon_i = \frac{\sqrt{\frac{1}{\tau}\sum_{j=t}^{t+\tau-1}\left[N_i(j)-\widehat{N}_i(j)\right]^2}}{\sqrt{\frac{1}{\tau}\sum_{j=t}^{t+\tau-1}\left[N_i(j)-N_i(t-1)\right]^2}}, \quad (4)$$

where $\tau = 3$ is the number of forecasts, the numerator is the RMSE for the LSTM neural network forecast ($\widehat{N}_i(j)$), and the denominator is the RMSE for a naive forecast using the last point in the current training set ($N_i(t-1)$). We then compute the rank correlation (ρ) between $\mathbb{E}(s_i)$ and ϵ_i as well as between $|\mathbf{v}_{1i}|$ and ϵ_i at each point in the test set to test the hypothesis that our rankings can predict the order of forecast errors. We also compute the rank correlation between each of the two alternative indicators previously described ($\Delta N_i(t)$ and $-N_i(t)$) and ϵ_i to verify whether these single-species indicators can predict the order of forecast errors. Because we do not know how perturbations affect these communities, we set $\mathbf{\Sigma}_t = \mathbf{I}$ and $k = \tau$ to compute $\mathbb{E}(s_i)$ (Box 1). We confirm the rationale behind

our hypothesis by performing forecasts under perturbations with the five models used in our theoretical analyses (Figure S19; SI Section 8).

We first illustrate our approaches to detect sensitive species with a rocky intertidal community. We find that barnacles have the highest expected sensitivity ($\mathbb{E}(s_i)$) followed by either algae or mussels depending on the point in time (Figure 4a and Figure S20). Interestingly, barnacles also show the highest alignment with the leading eigenvector ($|\mathbf{v}_{1i}|$) for the majority of points in time (Figure S20). We also find consistent results for $\mathbb{E}(s_i)$ and $|\mathbf{v}_{1i}|$ with a marine plankton community (Figures S20 and S21). Thus, although the values of $\mathbb{E}(s_i)$ over time are different from those of $|\mathbf{v}_{1i}|$, these two complementary approaches suggest some general patterns in how species sensitivities change over time in these two communities. Importantly, we find that the mean rank correlation $\overline{\rho}$ between $\mathbb{E}(s_i)$ and ϵ_i is positive for both time series, but only significant for one of them (rocky intertidal community: $\overline{\rho} = 0.04$, p-value = 0.287, 1000 randomizations; marine plankton community: $\overline{\rho} = 0.23$, p-value <0.001; Figure 4b). However, we find that the mean rank correlation $\overline{\rho}$ between $|\mathbf{v}_{1i}|$ and ϵ_i is positive and significant for both

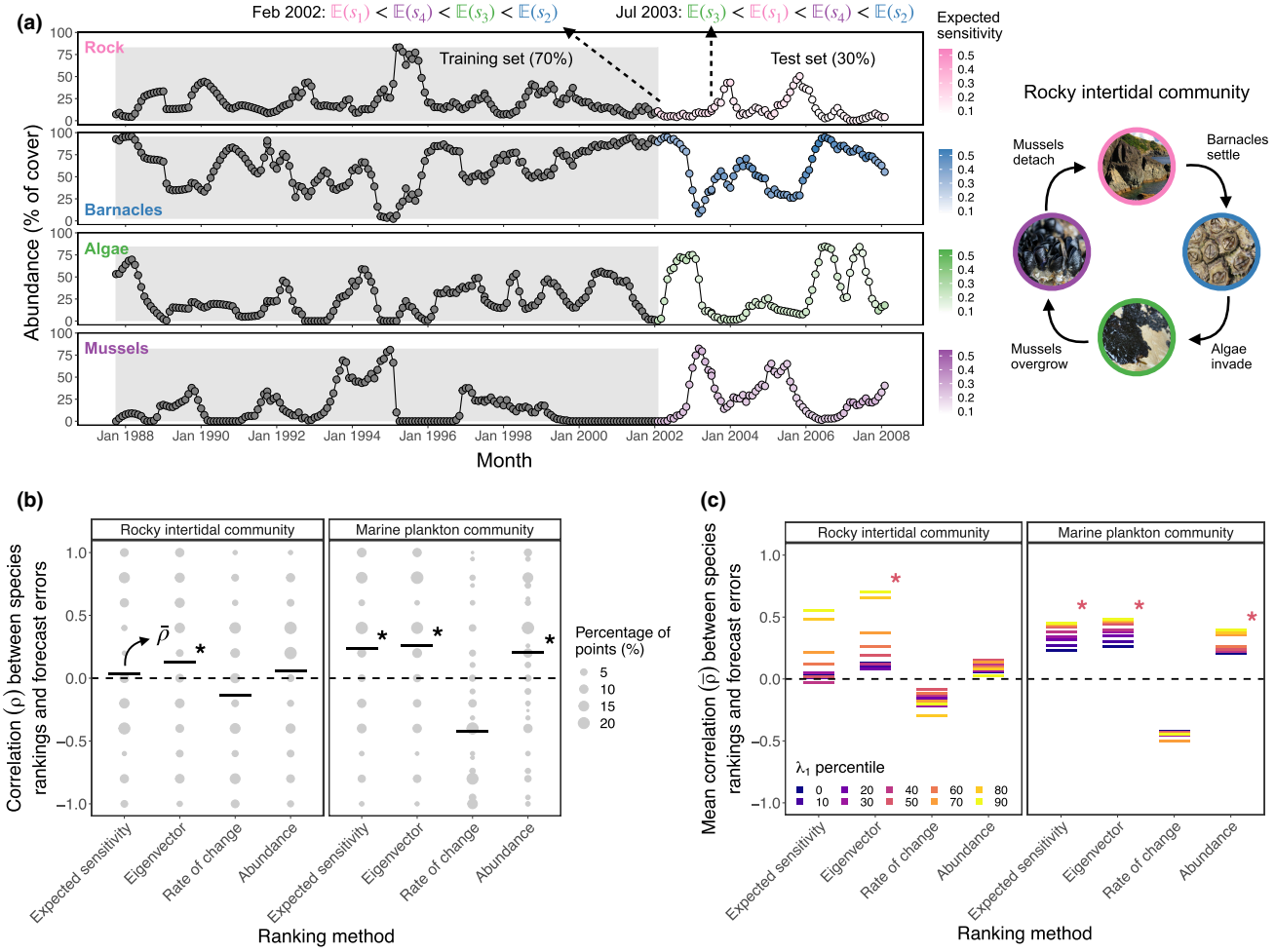

FIGURE 4 Species abundance forecast errors are associated with species sensitivities to perturbations. (a) Time series of a rocky intertidal community containing four variables (bare rock, barnacles, algae, and mussels). The diagram on the right depicts the cyclic succession in this community (adapted from Benincà et al., 2015). Note that percentage of cover does not necessarily sum to 100% as individuals of different species may overlap on top of the rock. We use a moving training set (grey region) to train the S-map and compute expected sensitivities ($\mathbb{E}(s_i)$) as well as species alignments with the leading eigenvector ($|\mathbf{v}_{1i}|$) at the last point in the training set. Simultaneously, we train an LSTM neural network to forecast species abundances and compute species forecast errors (ϵ_i). Barnacles (blue) show the highest value of $\mathbb{E}(s_i)$ followed by either algae (green) or mussels (purple) depending on the point in time. Note that $\mathbb{E}(s_i)$ values across species sum to 1 for each point in time (darker points denote higher $\mathbb{E}(s_i)$). (b) Rank correlation (ρ) between ϵ_i and four different approaches (expected sensitivity, $\mathbb{E}(s_i)$; eigenvector, $|\mathbf{v}_{1i}|$; rate of change, $\Delta N_i(t)$; and abundance, $-N_i(t)$). Each panel shows the percentage of points with a given ρ value (size of grey points) and the average of these values over the test set ($\overline{\rho}$, black horizontal lines) for a given empirical time series (asterisks denote a p-value less than 0.05 for $\overline{\rho}$ according to a randomization test). (c) Average correlation ($\overline{\rho}$) between ϵ_i and the different ranking approaches computed for points in the test set with a λ_1 value higher than a given percentile of the λ_1 distribution. For the expected sensitivity and eigenvector approaches, $\overline{\rho}$ increases as we only use points with successively higher values of λ_1 for both time series (asterisks denote a p-value less than 0.05 for $\overline{\rho}$ using the 50th percentile). Pictures are under the creative commons Licence: Rock by Piotr Zurek, barnacles by tangatawhenua, algae by redrovertracy, and mussels by Wayne Martin.

time series (rocky intertidal community: $\overline{\rho} = 0.13$, p-value = 0.023; marine plankton community: $\overline{\rho} = 0.26$, p-value <0.001; Figure 4b).

We find further evidence that species with higher $\mathbb{E}(s_i)$ or $|\mathbf{v}_{1i}|$ are harder to forecast by computing $\overline{\rho}$ only for points in the test set with successively higher values of λ_1 (i.e. higher local growth rate of perturbations; Figure 4c). For example, as expected from our analyses with synthetic time series (Figure S7), $\overline{\rho}$ between $|\mathbf{v}_{1i}|$ and ϵ_i increases for both time series when we only use points for which λ_1 is higher than its 50th percentile (rocky intertidal community: $\overline{\rho} = 0.19$, p-value = 0.021; marine plankton community: $\overline{\rho} = 0.45$, p-value <0.001; Figure 4c). The fact that $\overline{\rho}$ does not increase in general by using only points with a high λ_1 for the alternative indicators ($\Delta N_i(t)$ and $-N_i(t)$) supports our ranking approaches in linking species forecast errors to their sensitivities (Figure 4c). We find these results to remain similar when changing the size of the training set and the number of steps ahead (τ) to forecast (Figures S22–S24) as well as to normalize species abundances before performing the S-map (Figure S25).

DISCUSSION

Understanding how individual species affect the response to perturbations of the whole community and, in turn, how species interactions at the community level affect the responses of individual species is paramount to ecological management and conservation (Beauchesne et al., 2021; Clark et al., 2021; Kéfi et al., 2019; Levin & Lubchenco, 2008). Yet, the traditional focus of ecology on recovery to equilibrium using parameterized models has hampered efforts to understand how species respond to perturbations when community dynamics are out of equilibrium. Here, we introduce a data-driven framework to solve a previously unexplored problem: how to rank the species that compose a community according to their sensitivity to small pulse perturbations under non-equilibrium dynamics? Our findings provide three main insights into how communities and their constituent species respond to perturbations.

First, we show that information on the time-varying local effects between interacting species (i.e. Jacobian matrix) can be used to determine which species will be most affected by perturbations at a given time. In particular, using dynamical systems theory (Arnoldi et al., 2018; Mease et al., 2003; Strogatz, 2018) and nonlinear time series methods (Cenci et al., 2019; Deyle et al., 2016; Sugihara, 1994), we develop two complementary approaches that can accurately rank species from most to least sensitive to small perturbations on abundances under non-equilibrium dynamics. Both the expected sensitivity and the eigenvector ranking allow us to detect which of the species that compose a natural community are the most and least sensitive in real time if a long-time series is available. Hence, it may be possible to inform management and conservation programs regarding which species are currently the most sensitive ones. Our measure of sensitivity uses community-level information to quantify the likelihood of large changes (either decreases or increases) in the abundance of a given species. Therefore, species sensitivities may complement indicators that estimate single-species vulnerability to perturbations (Caswell, 2000; Mace et al., 2008; Morris & Doak, 2002). That is, whilst some species obviously require constant monitoring due to a high extinction risk (Dirzo et al., 2014; Estes et al., 2011), other species may require more attention during periods of time when they have a high sensitivity, irrespective of their abundance. Our results, however, cannot be extrapolated beyond a given studied community as our framework uses information on that specific community to rank species sensitivities.

Importantly, the expected sensitivity ranking is more accurate than the eigenvector ranking for most of our perturbation analyses with synthetic time series. In particular, the expected sensitivity ranking has its best performance when the time over which perturbations evolve (k) is small and fixed, and its worse performance when the covariance matrix of perturbations ($\mathbf{\Sigma}_t$) and k are greatly misspecified. In contrast, the eigenvector ranking has the advantage of not depending on $\mathbf{\Sigma}_t$ and k for its computation and has its best performance when k depends on the local time scale of the dynamics. Indeed, in communities under non-equilibrium dynamics, large differences in time scale and, therefore, in the time it takes for perturbation effects to appear are widespread (Hastings et al., 2018; Rinaldi & Scheffer, 2000; Strogatz, 2018). Thus, it is reasonable to expect that as a practical tool the heuristic eigenvector ranking may be as useful as the more theoretically complete but assumption bound expected sensitivity ranking.

Second, we find support for our hypothesis that the abundance forecast errors for the different species in a community are associated with their sensitivity to perturbations. The predictability of ecological dynamics is known to change across communities (Dietze, 2017; Pennekamp et al., 2019) and, for a single community, across time (Cenci et al., 2020). In particular, it has been shown that at points in time when a community is more sensitive to perturbations its local predictability can be lower and, therefore, the average abundance forecast error can be higher (Cenci et al., 2020). Here, we have extended this result for individual species by showing that the local predictability of a given species is associated with its sensitivity to perturbations, which we infer through its expected sensitivity and its alignment with the leading eigenvector. The fact that the correlation between forecast errors and our ranking approaches strengthens when the leading eigenvalue is high (i.e. perturbations grow rapidly along a given direction in state space) further supports our hypothesis that species forecast errors are associated with their sensitivities. In

addition, the better performance with empirical data of the eigenvector approach in relation to the expected sensitivity approach suggests that we may be misspecifying the information required to compute expected sensitivities. These results provide empirical support to the leading eigenvector as a way to detect sensitive species using minimal information inferred from time-series data. Overall, our findings suggest that sensitivity to perturbations is an additional factor influencing the intrinsic predictability of different species in ecological communities (Dietze, 2017, Pennekamp et al., 2019).

Applying our ranking approaches to empirical data requires accurate inference of the Jacobian matrix with the S-map. Although the S-map has been shown to provide accurate inferences when time series are noisy (Cenci et al., 2019; Deyle et al., 2016), several limitations remain. Because information on the shape of the attractor is required to fit the S-map, longer time series with smaller amounts of noise improve inference quality, all else being equal. In our analyses with synthetic time series, we show that our ranking approaches remain accurate when using shorter time series (Figure S16) or under small amounts of noise (Figures S17 and S18). Long time series with a strong signal of non-equilibrium deterministic dynamics, such as the rocky intertidal or plankton community investigated here (Benincà et al., 2009, 2015), are examples of ideal data sets to apply our approaches. Thus, even if small perturbations are continually impacting the community (e.g. ongoing process noise), if the attractor is not completely distorted, the S-map should be able to accurately reconstruct the time-varying Jacobian matrix required to compute species sensitivities (Cenci et al., 2019) (Figure S18). Although here we focus on small communities and small amounts of noise, future work may combine our ranking approaches with recent improvements in the S-map (e.g. regularization and multiview distance; Cenci et al., 2019; Chang et al., 2021) to detect sensitive species under more challenging settings.

Finally, we show that approaches based on linear dynamical systems that are typically used for communities close to equilibrium can also provide information for communities under non-equilibrium dynamics (Cenci & Saavedra, 2019; Ushio et al., 2018). Even though the methodology may be similar in both cases, the interpretation is completely different. For instance, whereas the linearized dynamics can be used to compute a recovery rate under equilibrium (Arnoldi et al., 2018; Medeiros et al., 2021; Strogatz, 2018), we show that they can be used to derive the time-varying expected sensitivity of different species to perturbations under non-equilibrium dynamics. In addition, we use the leading eigenvector, which has been previously employed to decompose community responses into species responses to perturbations under equilibrium dynamics (Dakos, 2018; Ghadami et al., 2020; Patterson et al., 2021; Weinans et al., 2019). Therefore, the approaches introduced here to increase our understanding of how communities and their constituent species respond to perturbations when there is no stable equilibrium. Both approaches are based on a linearization of the dynamics and, thereby, only provide an assessment of responses to small perturbations. Moreover, both approaches assume that the Jacobian matrix does not change much over the time period for which perturbations evolve. Improving our framework to deal with strong nonlinearities, fast changes in the Jacobian matrix and local oscillations due to complex eigenvalues are promising avenues for future research. As our knowledge of the impact of perturbations on a community increases, it might also be possible to incorporate biased (e.g. certain species are more impacted) or correlated (e.g. certain species are impacted in the same way) perturbation distributions into our approaches. Overall, our findings illustrate how integrating well-known results of equilibrium dynamics with data-driven methods for non-equilibrium dynamics provides a fruitful avenue for future development and new insights into the response of single species and entire communities to perturbations.

AUTHOR CONTRIBUTIONS

Lucas P. Medeiros and Serguei Saavedra designed research with inputs from Stefano Allesina, Vasilis Dakos and George Sugihara; Lucas P. Medeiros performed analyses; Serguei Saavedra supervised the study; Lucas P. Medeiros and Serguei Saavedra wrote the paper with substantial revisions from Stefano Allesina, Vasilis Dakos and George Sugihara.

ACKNOWLEDGEMENTS

We thank D. Rothman, T. Lieberman, S. Cenci, C. Song, J. Deng, and M. AlAdwani for insightful discussions and suggestions regarding this work. We also thank the reviewers and editor for suggestions that improved our paper. L.P.M. was supported by MIT ESI and the Martin Family Society of Fellows for Sustainability. G.S. was supported by DoD-Strategic Environmental Research and Development Program 15 RC-2509, NSF DEB-1655203, NSF ABI-1667584, and DOI USDI-NPS P20AC00527. S.S. was supported by NSF DEB-2024349 and the MIT Sea Grant Program.

CONFLICT OF INTEREST

The authors declare no competing interests.

PEER REVIEW

The peer review history for this article is available at https://publons.com/publon/10.1111/ele.14131.

DATA AVAILABILITY STATEMENT

The data and code supporting the results are archived on Github (https://github.com/lucaspdmedeiros/ranking-species-sensitivity) and Zenodo (https://doi.org/10.5281/zenodo.7120866).

ORCID

Lucas P. Medeiros https://orcid.org/0000-0002-0320-5058
Stefano Allesina https://orcid.org/0000-0003-0313-8374
Vasilis Dakos https://orcid.org/0000-0001-8862-718X
George Sugihara https://orcid.org/0000-0002-2863-6946
Serguei Saavedra https://orcid.org/0000-0003-1768-363X

REFERENCES

Aparicio, A., Velasco-Hernández, J.X., Moog, C.H., Liu, Y.Y. & Angulo, M.T. (2021) Structure-based identification of sensor species for anticipating critical transitions. *Proceedings of the National Academy of Sciences of the United States of America*, 118, e2104732118.

Arnoldi, J.F., Bideault, A., Loreau, M. & Haegeman, B. (2018) How ecosystems recover from pulse perturbations: a theory of short-to long-term responses. *Journal of Theoretical Biology*, 436, 79–92.

Barlow, J., França, F., Gardner, T.A., Hicks, C.C., Lennox, G.D., Berenguer, E. et al. (2018) The future of hyperdiverse tropical ecosystems. *Nature*, 559, 517–526.

Bartomeus, I., Saavedra, S., Rohr, R.P. & Godoy, O. (2021) Experimental evidence of the importance of multitrophic structure for species persistence. *Proceedings of the National Academy of Sciences of the United States of America*, 118, e2023872118.

Beauchesne, D., Cazelles, K., Archambault, P., Dee, L.E. & Gravel, D. (2021) On the sensitivity of food webs to multiple stressors. *Ecology Letters*, 24, 2219–2237.

Bender, E.A., Case, T.J. & Gilpin, M.E. (1984) Perturbation experiments in community ecology: theory and practice. *Ecology*, 65, 1–13.

Benincà, E., Ballantine, B., Ellner, S.P. & Huisman, J. (2015) Species fluctuations sustained by a cyclic succession at the edge of chaos. *Proceedings of the National Academy of Sciences of the United States of America*, 112, 6389–6394.

Benincà, E., Jöhnk, K.D., Heerkloss, R. & Huisman, J. (2009) Coupled predator–prey oscillations in a chaotic food web. *Ecology Letters*, 12, 1367–1378.

Boyce, W.E., DiPrima, R.C. & Meade, D.B. (2017) *Elementary differential equations*. Hoboken, NJ: John Wiley & Sons.

Cardinale, B.J., Duffy, J.E., Gonzalez, A., Hooper, D.U., Perrings, C., Venail, P. et al. (2012) Biodiversity loss and its impact on humanity. *Nature*, 486, 59–67.

Caswell, H. (2000) *Matrix population models*, Vol. 1. Sunderland, MA: Sinauer.

Cenci, S., Medeiros, L.P., Sugihara, G. & Saavedra, S. (2020) Assessing the predictability of nonlinear dynamics under smooth parameter changes. *Journal of the Royal Society Interface*, 17, 20190627.

Cenci, S. & Saavedra, S. (2019) Non-parametric estimation of the structural stability of non-equilibrium community dynamics. *Nature Ecology & Evolution*, 3, 912–918.

Cenci, S., Sugihara, G. & Saavedra, S. (2019) Regularized s-map for inference and forecasting with noisy ecological time series. *Methods in Ecology and Evolution*, 10, 650–660.

Chang, C.W., Miki, T., Ushio, M., Ke, P.J., Lu, H.P., Shiah, F.K. et al. (2021) Reconstructing large interaction networks from empirical time series data. *Ecology Letters*, 24, 2763–2774.

Clark, A.T., Arnoldi, J.F., Zelnik, Y.R., Barabas, G., Hodapp, D., Karakoç, C. et al. (2021) General statistical scaling laws for stability in ecological systems. *Ecology Letters*, 24, 1474–1486.

Clark, T. & Luis, A.D. (2020) Nonlinear population dynamics are ubiquitous in animals. *Nature Ecology & Evolution*, 4, 75–81.

Dakos, V. (2018) Identifying best-indicator species for abrupt transitions in multispecies communities. *Ecological Indicators*, 94, 494–502.

Deyle, E.R., May, R.M., Munch, S.B. & Sugihara, G. (2016) Tracking and forecasting ecosystem interactions in real time. *Proceedings of the Royal Society B: Biological Sciences*, 283, 20152258.

Dietze, M.C. (2017) *Ecological forecasting*. Princeton, NJ: Princeton University Press.

Dirzo, R., Young, H.S., Galetti, M., Ceballos, G., Isaac, N.J. & Collen, B. (2014) Defaunation in the anthropocene. *Science*, 345, 401–406.

Domínguez-García, V., Dakos, V. & Kéfi, S. (2019) Unveiling dimensions of stability in complex ecological networks. *Proceedings of the National Academy of Sciences of the United States of America*, 116, 25714–25720.

Eckmann, J.P. & Ruelle, D. (1985) Ergodic theory of chaos and strange attractors. In: Hunt, B.R., Li, T.Y., Kennedy, J.A. & Nusse, H.E. (Eds.) *The theory of chaotic attractors*. New York, NY: Springer, pp. 273–312.

Estes, J.A., Terborgh, J., Brashares, J.S., Power, M.E., Berger, J., Bond, W.J. et al. (2011) Trophic downgrading of planet earth. *Science*, 333, 301–306.

Ghadami, A., Chen, S. & Epureanu, B.I. (2020) Data-driven identification of reliable sensor species to predict regime shifts in ecological networks. *Royal Society Open Science*, 7, 200896.

Hastings, A., Abbott, K.C., Cuddington, K., Francis, T., Gellner, G., Lai, Y.C. et al. (2018) Transient phenomena in ecology. *Science*, 361, eaat6412.

Hastings, A. & Powell, T. (1991) Chaos in a three-species food chain. *Ecology*, 72, 896–903.

Ives, A.R., Gross, K. & Klug, J.L. (1999) Stability and variability in competitive communities. *Science*, 286, 542–544.

Jackson, J.B., Kirby, M.X., Berger, W.H., Bjorndal, K.A., Botsford, L.W., Bourque, B.J. et al. (2001) Historical overfishing and the recent collapse of coastal ecosystems. *Science*, 293, 629–637.

James, G., Witten, D., Hastie, T. & Tibshirani, R. (2021) *An introduction to statistical learning: with applications in R*. New York, NY: Springer.

Kéfi, S., Domnguez-Garca, V., Donohue, I., Fontaine, C., Thébault, E. & Dakos, V. (2019) Advancing our understanding of ecological stability. *Ecology Letters*, 22, 1349–1356.

Krebs, C.J., Boutin, S., Boonstra, R., Sinclair, A., Smith, J., Dale, M.R. et al. (1995) Impact of food and predation on the snowshoe hare cycle. *Science*, 269, 1112–1115.

Kuptsov, P.V. & Parlitz, U. (2012) Theory and computation of covariant lyapunov vectors. *Journal of Nonlinear Science*, 22, 727–762.

Lever, J.J., van de Leemput, I.A., Weinans, E., Quax, R., Dakos, V., van Nes, E.H. et al. (2020) Foreseeing the future of mutualistic communities beyond collapse. *Ecology Letters*, 23, 2–15.

Levin, S.A. & Lubchenco, J. (2008) Resilience, robustness, and marine ecosystem-based management. *BioScience*, 58, 27–32.

Mace, G.M., Collar, N.J., Gaston, K.J., Hilton-Taylor, C., Akçakaya, H.R., Leader-Williams, N. et al. (2008) Quantification of extinction risk: IUCN's system for classifying threatened species. *Conservation Biology*, 22, 1424–1442.

Mease, K., Bharadwaj, S. & Iravanchy, S. (2003) Timescale analysis for nonlinear dynamical systems. *Journal of Guidance, Control, and Dynamics*, 26, 318–330.

Medeiros, L.P., Song, C. & Saavedra, S. (2021) Merging dynamical and structural indicators to measure resilience in multispecies systems. *Journal of Animal Ecology*, 90, 2027–2040.

Morris, W.F. & Doak, D.F. (2002) *Quantitative conservation biology*. Sunderland, MA: Sinauer.

Patterson, A.C., Strang, A.G. & Abbott, K.C. (2021) When and where we can expect to see early warning signals in multispecies systems approaching tipping points: insights from theory. *The American Naturalist*, 198, E12–E26.

Pennekamp, F., Iles, A.C., Garland, J., Brennan, G., Brose, U., Gaedke, U. et al. (2019) The intrinsic predictability of ecological time series and its potential to guide forecasting. *Ecological Monographs*, 89, e01359.

Perretti, C.T., Munch, S.B. & Sugihara, G. (2013) Model-free forecasting outperforms the correct mechanistic model for simulated

and experimental data. *Proceedings of the National Academy of Sciences of the United States of America*, 110, 5253–5257.
Rinaldi, S. & Scheffer, M. (2000) Geometric analysis of ecological models with slow and fast processes. *Ecosystems*, 3, 507–521.
Rogers, T.L., Johnson, B.J. & Munch, S.B. (2022) Chaos is not rare in natural ecosystems. *Nature Ecology & Evolution*, 6, 1–7.
Saavedra, S., Stouffer, D.B., Uzzi, B. & Bascompte, J. (2011) Strong contributors to network persistence are the most vulnerable to extinction. *Nature*, 478, 233–235.
Song, C. & Saavedra, S. (2021) Bridging parametric and nonparametric measures of species interactions unveils new insights of non-equilibrium dynamics. *Oikos*, 130, 1027–1034.
Strogatz, S.H. (2018) *Nonlinear dynamics and chaos: with applications to physics, biology, chemistry, and engineering*. Boulder, CO: Westview Press.
Sugihara, G. (1994) Nonlinear forecasting for the classification of natural time series. *Philosophical Transactions of the Royal Society of London. Series A: Physical and Engineering Sciences*, 348, 477–495.
Turner, M.G., Dale, V.H. & Everham, E.H. (1997) Fires, hurricanes, and volcanoes: comparing large disturbances. *BioScience*, 47, 758–768.
Ushio, M., Hsieh, C.H., Masuda, R., Deyle, E.R., Ye, H., Chang, C.W. et al. (2018) Fluctuating interaction network and time-varying stability of a natural fish community. *Nature*, 554, 360–363.
Vallejo, J.C., Sanjuan, M.A. & Sanjuán, M.A. (2017) *Predictability of chaotic dynamics*. Cham, Switzerland: Springer.
Weinans, E., Lever, J.J., Bathiany, S., Quax, R., Bascompte, J., Van Nes, E.H. et al. (2019) Finding the direction of lowest resilience in multivariate complex systems. *Journal of the Royal Society Interface*, 16, 20190629.

SUPPORTING INFORMATION

Additional supporting information can be found online in the Supporting Information section at the end of this article.

How to cite this article: Medeiros, L.P., Allesina, S., Dakos, V., Sugihara, G. & Saavedra, S. (2022) Ranking species based on sensitivity to perturbations under non-equilibrium community dynamics. *Ecology Letters*, 00, 1–14. Available from: https://doi.org/10.1111/ele.14131